The effect of dielectric spacer thickness on surface plasmon enhanced solar cells for front and rear side depositions

S. Pillai,[1,a)] F. J. Beck,[2] K. R. Catchpole,[2] Z. Ouyang,[1] and M. A. Green[1]
[1]*ARC Photovoltaics Centre of Excellence, University of New South Wales, Sydney, NSW 2052, Australia*
[2]*Center for Sustainable Energy Systems, College of Engineering and Computer Science, Australian National University, Canberra ACT 0200, Australia*

(Received 13 September 2010; accepted 21 February 2011; published online 4 April 2011)

The excitation of surface plasmons on metallic nanoparticles has the potential to significantly improve the performance of solar cells, in particular thin-film structures. In this article, we investigate the effect of the dielectric spacer layer thickness on the photocurrent enhancement of 2 μm thick, thin-film poly-Si on glass solar cells, due to random arrays of self-assembled Ag nanoparticles deposited on the front or the rear of the cells. We report a strong asymmetry in the external quantum efficiency (EQE) of the cell for front and rear located particles for different spacer thicknesses, which is attributed to differences in the scattering behavior of the nanoparticles. We find that for random arrays, with spectrally broad scattering resonances, the strength of the driving field and the coupling efficiency are more important for light trapping than the resonance wavelength. For particles located on the front of the cells it is desirable to have a thin dielectric spacer layer to enhance the scattering from the Ag nanoparticles. Additionally, light trapping provided by the random sized particles on the front can overcome suppression of light transmitted in the visible wavelength regions for thin layers of Si, to result in overall EQE enhancements. However, for particles deposited on the rear it is more beneficial to have the particles as close to the Si substrate as possible to increase both the scattering and the coupling efficiency. © *2011 American Institute of Physics*. [doi:10.1063/1.3567299]

I. INTRODUCTION

Thin-film solar cells are regarded as the route to substantially reducing the cost of solar energy by reducing the material costs. Decreasing the semiconductor thickness not only contributes to cost reduction but can also potentially improve the open circuit voltage of the solar cells. As cells become thinner, light trapping becomes more important. Light trapping can be achieved by roughening the surface of the cells but highly scattering nanoscale texturing of the semiconductor is difficult to obtain and tends to also lead to increased surface recombination and reduced material quality, which can compromise the cell performance. To achieve a cost reduction and improve the electrical properties of thin Si films it would be advantageous to use wavelength scale light trapping that does not necessarily involve surface roughening. The field of plasmonics is a promising new way of providing light trapping in thin-film solar cells by exciting surface plasmons on metal nanoparticles.[1–4]

A major benefit of plasmonic light trapping lies in the fact that the metal nanoparticles can be deposited at the final stage of the device fabrication process without the need to change any processing conditions or compromise the material or surface quality. An added advantage is that the optical properties of the surface plasmons are decoupled from the electrical properties of the solar cell hence can be optimized independent of the cell structure.

II. BACKGROUND

Surface plasmons are known to be very sensitive to the refractive index of the dielectric medium within the penetration depth of the evanescent field. This forms the basis of their application in biosensors as a sensing transduction mechanism.[5] Thus, substrate effects form an important part of studying the plasmonic effect for solar cell applications. The coupling of the localized surface plasmons to an underlying substrate is also very sensitive to the spacing between the particles and the underlying substrate. For crystalline Si solar cells, the surface can represent the largest possible disturbance of the crystal lattice due to nonsaturated or dangling bonds allowing energy states in the forbidden bandgap. This can result in a recombination process via defect levels or surface states resulting in loss of light generated current and reduction in cell efficiency. For high efficiency crystalline Si cells it is imperative that a thin layer of dielectric like SiO_2 or Si_3N_4 be deposited on the Si to reduce surface recombination and improve the electrical properties of the device. Following this our earlier work made use of an arbitrary dielectric thickness of 20 nm which was the minimum needed to provide good surface passivation while maintaining reasonably high coupling of the scattered light into the underlying modes.[2,6] The sensitivity of plasmonic scattering to the local dielectric environment and the need to passivate the surface of solar cells motivates this study of the effect of spacer layer thickness on the scattering from the metal nanoparticles.

Placing a particle on a substrate can affect the scattering in three ways,[7] 1) modifying the polarizability of the particle, and hence the surface plasmon resonance wavelength, 2) changing the intensity of the electric field driving the surface plasmon resonance, and 3) changing the angular spectrum of the scattered light. All these effects are sensitively dependent on the details of the substrate geometry and the position of the particle.

a)Electronic mail: s.pillai@unsw.edu.au.

The first effect allows spectral tunability of the resonance of the particle to wavelength regions where transmission losses in Si solar cells become significant. The effect of the substrate on surface plasmons has been studied by many groups and the red shifting of the plasmon resonance wavelength with increasing refractive index of the substrate is well known.[8–10] The absorption coefficient of semiconductor materials drop close to its bandgap, hence shifting the resonance so that scattering occurs closer to the bandgap of the semiconductor material helps more light to be absorbed via light trapping. A higher refractive index medium like Si tends to red shift the resonance due to depolarization effects. This means that bringing the particles closer to the high index semiconductor by reducing the thickness of the spacer layer shifts the resonance to longer wavelengths, if the spacer layer thickness is similar to or smaller than the near-field of the surface plasmon excitation (a few tens of nm).

Secondly, the strength of the scattering cross section will also be modified by the thickness of the spacer layer,[11] due to changes in the electric field driving the resonance. The driving field increases with spacer layer thickness for particles located on the front, illuminated surface of the cell. This is closely related to the earlier work on the effect of substrates on dipole radiation, which was focused on the electromagnetic interactions of fluorescing molecules (treated as radiating dipoles) with metal surfaces.[12] Drexhage found that when a dipole is placed in front of a mirror, the path difference between the direct and reflected beam causes the molecules to radiate strongly when constructive interference occurs but suppresses radiation when interfering destructively. It has also been reported recently that particles located on the rear of substrates on ultra-thin spacer layers can have enhanced scattering cross-sections.[11]

Finally, the angular spectrum of the particle will be modified by the presence of a high refractive index substrate, leading to an asymmetric scattering profile. A large fraction of the scattered light will be coupled into the substrate and the exact fraction will be determined by the spacer layer thickness.[13] This ensures that more of the scattered light goes into the active semiconductor layer and is trapped by total internal reflection. This effect has been demonstrated in previous work, which showed that particles located on the front surface can provide anti-reflection and light trapping for solar cells.[2,14,15]

A few earlier studies have touched on the effect of spacer layers on the dipole properties of metal nanoparticles. Holland and Hall studied the effect of Ag metal nanoparticles in the presence of a metal surface and found that there is an optimum thickness of the spacer layer placed between the Ag nanoparticles and metal dielectric interface for maximum coupling which was found to be 25 nm for LiF and MgF_2 layers.[16] It has also been reported that for metal island films on thin Si waveguides, having a spacer layer helps to localize the waveguide mode field on the surface with the nanoparticles allowing better coupling with the plasmon modes.[17] Hagglund *et al*. describe reduced transmission for disk-shaped particles directly on an illuminated Si surface, which they attribute to a phase shift in the internal field for the upper and lower part of the disk shaped particle due to the asymmetry imposed by the interface.[18] They suggest having a thin spacer layer to reduce the phase difference.

Metal nanoparticles can absorb in the UV region of the spectrum and into the visible region as well, compromising the absorption in the Si. Below the resonance wavelength of the particles, a shift in the phase of the polarizability of the particle can lead to destructive interference between the incident and scattered light leading to a decrease in the photocurrent response.[19] This means that for photovoltaic applications, light in the spectral region below the resonance wavelength of the particle plasmons is not collected in the active regions of the cell, with the loss becoming more significant as we red shift the resonance to provide near bandgap light trapping. The advantage of having the metal nanoparticles on the rear is that only light that is not absorbed by the cell (transmitted light) would be exciting the plasmons. Even thin film Si cells normally absorb the short wavelength light strongly, hence any likely absorption in the metals or suppression of below resonance wavelengths can be avoided. Additionally, by tuning the surface plasmon resonance to longer wavelengths, the particles can be used to scatter more efficiently in the weakly absorbing regime without any compromise for visible regime absorption.

In this article, we investigate the effect of the dielectric layer thickness on the plasmonic light trapping provided by Ag nanoparticles, and its performance in thin-film Si solar cells. We systematically study the effect of Ag nanoparticle scattering for varying thickness of the oxide dielectric layer on the photocurrent and absorptance measurements, for both front and rear side depositions. Here it may be noted that most reports refer to front side nanoparticle depositions only as the advantages of having the particles on the rear has been realized experimentally only recently.[10,20,21] We demonstrate that spacer layer thickness should be optimized independently for front and rear located nanoparticles. We show that random arrays of particles on spacer layers of 20–30 nm provide good light trapping due to strong, broad scattering resonances, while particles directly on the Si on the rear of the cells provide the best enhancement. We demonstrate that the photocurrent suppression for front located particles can be compensated for at wavelengths where transmission losses occur, if the particles provide sufficient light trapping.

III. METHOD

Polycrystalline Si thin film solar cells deposited on glass and Si thin film samples on glass (which had not been processed into solar cells) were used for the investigation. To fabricate the samples, a 2 μm thick a-Si precursor layer was deposited by electron-beam evaporation onto planar borosilicate glass deposited with Si nitride. The PECVD deposited nitride layer serves as a diffusion barrier as well as an antireflection layer. The dopants are introduced *in situ* along with the Si deposition. The film structure consists of a thin phosphorus doped emitter followed by a boron-doped absorber (4×10^{15} cm^{-3}) and a back surface field (BSF). After deposition the films were crystallized, annealed, and hydrogen plasma passivated. The poly-Si cells were then metallized using interdigitated line contacts on both the emitter and the

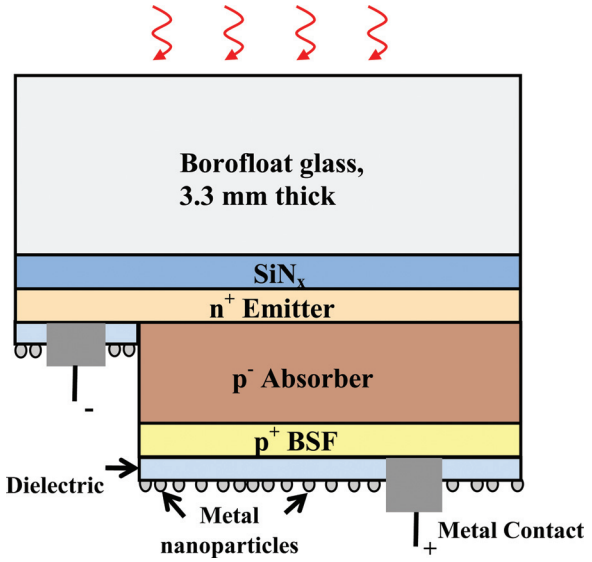

FIG. 1. (Color online) Schematic of the bifacial poly-Si evaporated cell used for the experiments.

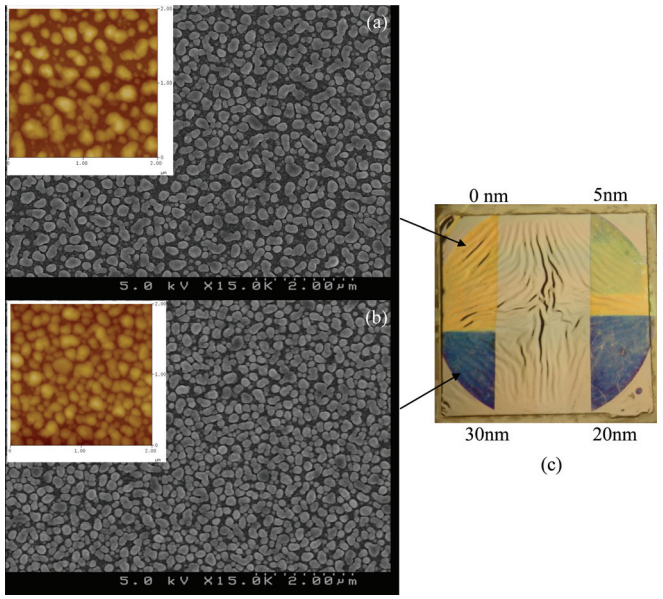

FIG. 2. (Color online) SEM images for particles on (a) Si and (b) 30 nm oxide with the respective AFM images shown in the inset. (c) The shifting of the surface plasmon resonance can be seen visually (in color print only), as shown in this photograph of Ag nanoparticles deposited under the same conditions on a crystalline Si on glass sample surface with different dielectric thicknesses of sputtered oxide. The dielectric thicknesses are (from top left in clockwise direction) 0 nm (yellow), 5 nm (green), 20 nm (blue), and 30 nm (deep blue).

absorber layers. More information on the fabrication and structural details of the evaporated cells can be found in Ref. 22. A thin nonstoichiometric layer of SiO_x of varying thickness was sputtered on some of the samples. Thicknesses of 30 nm were deposited for finished cells and 5, 20, and 30 nm were deposited for the plain thin film samples. The refractive index of the sputtered oxide was found to be around 1.6 from ellipsometry measurements. Metal nanoparticles were then deposited by thermally evaporating a 16 nm mass thickness of Ag and annealing it in flowing nitrogen for an hour at 200 °C on the finished solar cells (for electrical measurements) as well as the thin film samples (for optical measurements).

The thin-film evaporated poly-Si solar cells considered for this work are normally used in a glass superstrate configuration as shown in Fig. 1, and hence we have our nanoparticles deposited on the rear of the cell. For this illumination condition we refer to the particles as 'particles on the rear or rear located particles.' Conversely, the same structure when used in a glass substrate configuration with the emitter facing the air side, i.e., illumination is directed on to the nanoparticles, we refer it as 'particles on the front or front located particles.' The double sided measurements are possible because of the bifacial nature of the cell which enables us to measure the photocurrent with light incident from either side: with nanoparticles on the front or on the rear of the cells. The samples and nanoparticles used for each measurement are the same for both front and rear sides except that the illumination conditions are reversed.

The external quantum efficiency (EQE) of the thin Si solar cells was measured before and after the deposition of the Ag metal nanoparticles, to investigate the light trapping provided by nanoparticles on a 30 nm oxide spacer layer and with no oxide layer (native oxide only). EQE measures the ratio of the photo generated carriers (obtained from the measured current) to the incident photons as a function of wavelength. Optical measurements were performed on the thin film Si samples on glass substrates, with and without nanoparticle arrays on four different oxide spacer layer thicknesses of 0 nm, 5 nm, 20 nm, and 30 nm.

The poly-Si thin film solar cells have a very high bulk recombination rate due to defects and large grain boundaries. This together with the BSF makes any surface recombination contribution negligible. A sputtered oxide layer does not affect the electrical properties of the devices as evident from the comparison of EQE and *IV* curves before and after the deposition of the dielectric layer (not shown here). Therefore, any enhancement in photocurrent can be attributed to the presence of the metal nanoparticles. For this reason, the effect of the dielectric thickness can be studied without any dependence of surface recombination on spacer layer thickness.

SEM and AFM (inset) analysis of particles in Fig. 2(a) show that particles on Si have an average diameter between 150 and 250 nm with height of 40–60 nm. For particles on oxide for the same deposition as in Fig. 2(b), the average diameter is in the same range but they are flatter and more closely packed. The height from AFM analysis for these particles are around 30–40 nm. We find that the effect of the different average heights of the particles results in a slight red shifting of the scattering resonance peak (from numerical calculations described below) due to an increase in the aspect ratio. However, since the nanoparticles in the random arrays have a large size distribution and are randomly shaped, the overall effect on the scattering behavior, when averaged out over the array, will be negligibly small. As such, the dominant effect driving the trends seen experimentally will be due to the presence of the oxide layer and the change of spacer layer thickness.

Figure 2(c) shows the particles deposited on the different thickness of oxide and gives a visual representation of the resonance position for each case. The dielectric thicknesses are (from top left in clockwise direction) 0, 5, 20, and

30 nm. It can be clearly seen that the resonance wavelength is blue shifting from yellow to green, blue, and deep blue as the spacer layer thickness increases (visible in color print only). This is due the fact that a higher index surrounding like Si tends to red shift the plasmon resonance wavelength as discussed in Sec. V.

IV. RESULTS

A. Particles on the front

Figure 3(a) shows the EQE spectra for thin Si solar cells with Ag nanoparticle directly on the front surface, and separated from the Si active layer by a 30 nm oxide spacer layer. This was complemented with optical measurements of four plain Si thin-film samples with different thicknesses of oxide layer as described in Sec. III. Figure 3(b) shows optical absorptance spectra for particles on the front. For both cases data is also shown for cells and thin film samples without nanoparticles.

From Fig. 3(a) it is clearly evident that particles on the front on the oxide are performing better than particles directly on Si over the measured spectrum. The particles with an oxide increase the EQE from a wavelength of 600 to 1200 nm, while particles without the spacer layer are beneficial above 700 nm. Beyond wavelengths of 900 nm the enhancement is similar for both cases. The reduction in the cell response below 500 nm for the oxide case, and 650 nm for the no oxide case, is attributed to the suppression of the photocurrent response at wavelengths below resonance due to interference.[19] For particles on the front, the photocurrent suppression occurs at wavelengths below resonance due to destructive interference between incident and scattered light in the Si substrate. Above resonance, the particles are coupling light into the substrate in phase and there is enhancement. Front located nanoparticles on thicker spacer layers can increase the EQE over a wide wavelength range suitable for solar cells, while minimizing photocurrent suppression at sub-resonance wavelengths.

The absorptance measurements in Fig. 3(b) are in good agreement with the above EQE results in the wavelength region beyond 450 nm as the optical results below this wavelength can involve absorption in the Ag which cannot be isolated from absorption in the Si. The results show that particles on a relatively thick spacer layer of 20 to 30 nm provide greater absorption enhancement over a larger wavelength region, compared to particles directly on the Si and on ultra-thin spacer layers, 5 nm thick.

B. Particles on the rear

To measure the particles on the rear of the cells the direction of illumination was changed with the cell/sample having a glass superstrate configuration. Figure 4(a) shows EQE

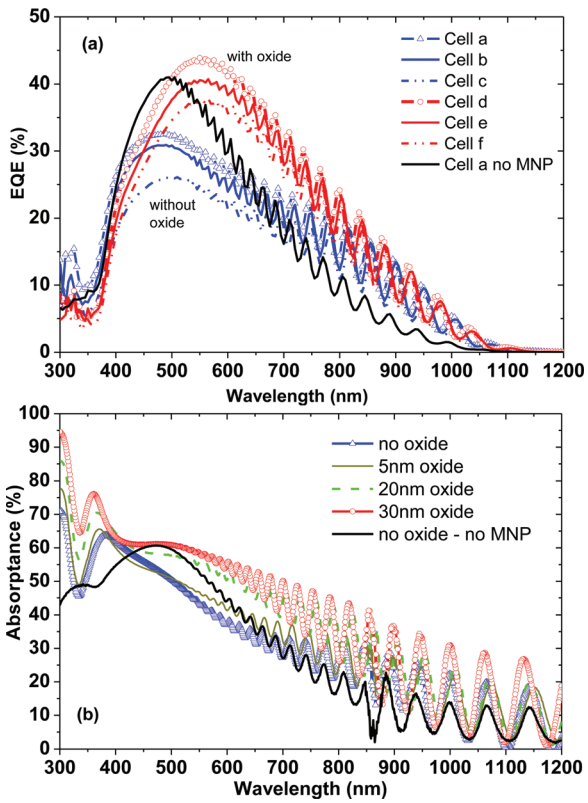

FIG. 3. (Color online) (a) The external quantum efficiency of 2 μm thick poly-Si cells deposited on glass for front side illumination. The blue plots (cells a, b, and c) are with no oxide layer, and the red plots (cells d, e, and f) are with 30 nm oxide (b) the corresponding optical absorptance from a similar sample with 0, 5, 20, and 30 nm of oxide. The solid black line in the two figures show the base measurements without dielectric and without any Si nanoparticles (MNP).

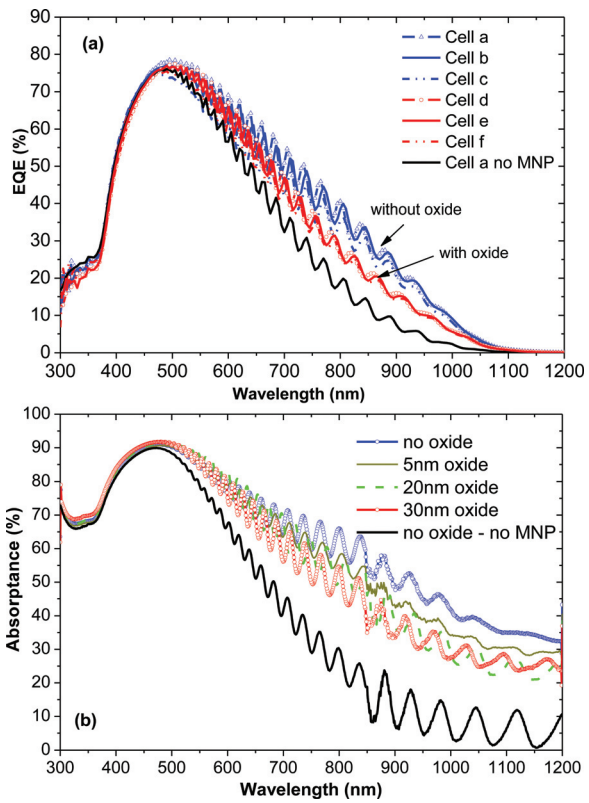

FIG. 4. (Color online) (a) The external quantum efficiency of 2 μm thick poly-Si cells deposited on glass for particles on the rear side. Solid lines (cells a, b, and c) are with no oxide layer and the dotted lines (cells d, e, and f) are with 30 nm oxide (b) the corresponding optical absorptance from a similar sample with 0, 5, 20, and 30 nm of oxide. The solid black line in the two figures show the base measurements without a dielectric layer and without any metal nanoparticles (MNP).

spectra for Si solar cells with and without nanoparticles on the rear surface of the solar cell. Results are shown for cells with and without a 30 nm oxide spacer layer. Figure 4(b) shows optical absorptance for thin Si films on glass, with and without nanoparticle arrays on varying thicknesses of oxide spacer layers.

From Figs. 4(a) and 4(b) it can be seen that all samples with particles on the rear, both on Si and on oxide layers, perform better than the case without any nanoparticles (black solid line) beyond 500 nm. This is because transmission losses begin to occur for a 2 μm thick Si cell above this wavelength, and hence the light trapping provided by the scattering layer results in an increase in photocurrent and absorptance. Unlike in Figs. 3(a) and 3(b), where particles are on the front of the cells, we do not observe any photocurrent suppression at short wavelengths. This is because at wavelengths below 500 nm the cell is thick enough to absorb the incoming light before it reaches the particles. The maximum EQE enhancement occurs for particles deposited directly on the Si surface, in agreement with results reported earlier for these cells.[20] What is interesting to note here is that the results follow a reverse trend when compared to the particles on the front.

V. DISCUSSION

To investigate the experimental results presented above, numerical simulations were performed using the FDTD solutions package from Lumerical.[23] These 3D simulations are purely optical and allow us to investigate the scattering behavior of the Ag particles. It is not possible to model the random arrays seen experimentally and so we instead use single particle simulations which have been shown to reproduce the trends seen in experimental results for random particle arrays.[10] The particles are located on semi-infinite Si substrates and the simulation volume is terminated with perfectly matched layer boundary conditions. The optical constants were calculated using a Drude model for Ag, fitted to optical data from Johnson and Christy[24] and a Drude–Lorentz model for Si, fitted to data from Keevers,[25] while the optical data for the oxide was taken from Palik.[26] The particle is illuminated with light incident from the air, corresponding to front located particles, or from the Si side, corresponding to rear located particles.

Simulations on semi-infinite substrates do not allow us to directly calculate the enhancement in absorption due to light trapping, however, we are able to calculate the scattering cross section and coupling efficiency of the particles. The normalized scattering cross-section can be thought of as the area over which the nanoparticles scatter light, and the coupling efficiency tells us how much of the scattered light ends up in the Si. These two parameters give us an indication of the amount of light coupled into the Si. A large fraction of this light will be traveling outside the loss cone (defined as the angle beyond which light is totally internally reflected) and will be trapped.

The modeled Ag nanoparticles have a truncated ellipsoidal shape with a total height of 55 nm (see inset Fig. 5). Three different diameters, corresponding to the most common particle sizes seen experimentally, were modeled for a semi-infinite substrate case. The particles are separated from the Si substrate by either a thin oxide spacer layer or a native oxide of 2.5 nm. The normalized scattering cross section Q_{scat}, is calculated by integrating the Poynting vector of the scattered field over a surface enclosing the particle and normalizing with respect to the intensity of the incident illumination, and the cross sectional area of the particle. The scattered power can be calculated separately in the substrate and in the air. The coupling efficiency is then quantified by calculating the fraction of the scattered power that is scattered into the substrate, and is denoted by F_{subs}.

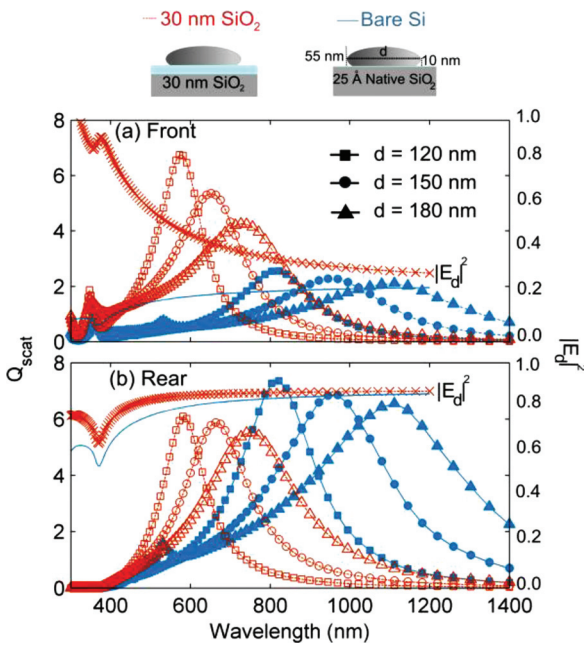

FIG. 5. (Color online) Calculated Q_{scat} for Ag particles with a truncated ellipsoidal shape of height 55 nm and of varying diameter, d = 120 (squares), 150 (circles), and 180 nm (triangles). The particles are separated from Si substrates by either 30 nm oxide (red, open markers) or bare Si (blue, solid markers) with a 2.5 nm native oxide. Data is shown for (a) front located and (b) rear located particles. The calculated $|E_d|^2$ is also plotted for front and rear located particles with (red, dashed line, crosses) and without a spacer layer (blue, solid line).

As mentioned in the background section, the electric field driving the surface plasmon excitation in the nanoparticles is modified due to the presence of the layered substrate and is dependent on the location of the nanoparticle. The driving field, E_d, at the position of the particle illuminated from the air (front located particles) is therefore a superposition of the incident field and the field reflected back from the interface. For a particle illuminated from the Si substrate (rear located particle), the driving field is given by the field transmitted at the interface. The normalized driving field intensity, $|E_d|^2$ can be calculated for a Si substrate in air, with and without a 30 nm oxide layer, using a simple analytical model for a semi-infinite substrate, as described in Ref. 11.

Figure 5 shows the calculated Q_{scat} for the Ag particles, with (open markers) and without (solid markers) a 30 nm spacer layer, for (a) front located particles and (b) rear-located particles. The normalized driving field intensity, $|E_d|^2$ is plotted on the same figure for comparison (on oxide: red

dashed lines with crosses; on Si: solid blue line). On the front, in Fig. 5(a), the resonances of the particles occur at wavelengths of 800 to 1200 nm on bare Si, and are blue-shifted to between 600 and 800 nm on the oxide. This is due to a reduction in the depolarization effects due to the Si substrate as the spacer layer increases, and is consistent with the blue shifting of color seen experimentally in Fig. 2(c). Additionally, the resonances on the oxide are roughly twice as strong due to the increased normalized driving field intensity at resonance. For example, the strength of the Q_{scat} at resonance is 2.3 times that of the bare Si for the 150 nm diameter particle, and the corresponding ratio of $|E_d|^2$ at resonance is equal to 1.9. This is in agreement with results reported in Ref. 11.

On the rear, the resonances occur at the same wavelengths as on the front, as expected. However, the peak value of Q_{scat} at resonance is different. Now, the strength of the resonance is 35% larger on the bare Si at a wavelength of 822 nm, compared to the resonance of particles on an oxide, at 756 nm, despite the fact that the normalized driving field intensity is 3.6% higher with the 30 nm oxide present. Again, this is consistent with results in Ref. 11, where we reported an enhanced Q_{scat} for rear located particles on bare Si.

Figure 6 shows the calculated F_{subs} for 150 nm diameter particles on bare Si, with only a 2.5 nm native oxide, and separated from the substrate by a 30 nm oxide spacer layer. We can see that the shape asymmetry does not result in significant differences in the coupling efficiency between front and rear located particles. For particles directly on the Si the F_{subs} converges to 95% for wavelengths beyond 800 nm, where the scattering resonance occurs. However, for particles on 30 nm oxide spacer layers the coupling efficiency is reduced to 80–90% at wavelengths at which resonance occurs, i.e., between 600 to 800 nm, due to the reduced overlap of the near field of the particle with the substrate.[13]

We now relate the scattering behavior of the particles to the experimental results. Figure 7 shows experimental EQE enhancement results calculated from Figs. 3(a) and 4(a) for the case with (cell d) and without (cell a) the oxide. The enhancement is the ratio of the EQE after the deposition of the particles to that of a bare cell. First, we will concentrate on the long wavelength region, from 600 to 1200 nm. The experimental enhancements plotted in Fig. 7(a) show that from a wavelength of 600 nm up to 900 nm we get larger

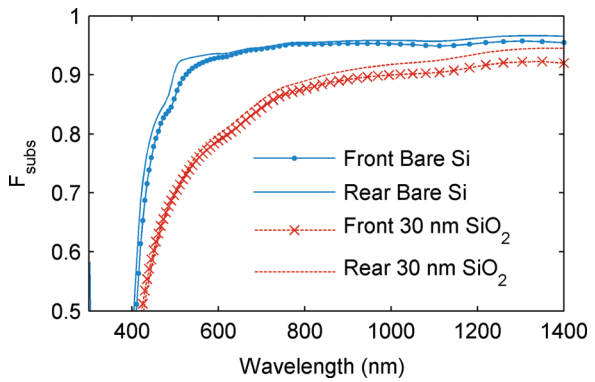

FIG. 6. (Color online) Calculted F_{subs} for 150 nm nanoparticles on bare Si, with only a 2.5 nm native oxide, and separated from the substrate by a 30 nm oxide spacer layer.

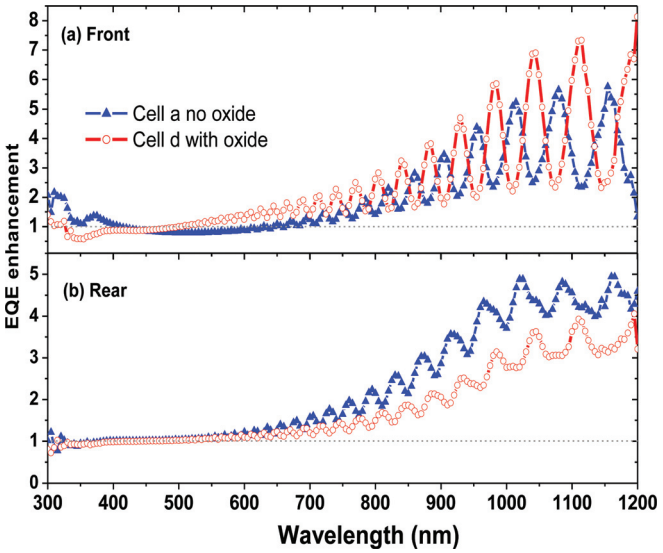

FIG. 7. (Color online) EQE enhancement plots for particles in the (a) front and (b) rear for the case with (cell d) and without (cell a) the oxide layer.

enhancements due to front located nanoparticles on an oxide, compared to particles on bare Si. We have reported previously[2] that self-assembled arrays of nanoparticles, formed from 16 nm thick Ag films on glass slides, have resonances that peak at a wavelength of 500 nm and extend out to 1200 nm (Fig. 2 in Ref. 2). Hence, experimentally we would expect the collective resonances of the random particle arrays to be very broad. In the spectral region from 600 to 1200 nm, the relative size of Q_{scat} on bare Si, and with oxide spacer layers, is then determined by the strength of the driving field, rather than the resonance position.

On the front of Si substrates, as shown in Fig. 5(a), particles on an oxide have larger driving field intensities for all wavelengths. For example, at a wavelength of 750 nm we can estimate that Q_{scat} is almost twice as large due to the oxide compared to the bare Si case from the ratio of $|E_d|^2 = 3.39/1.75$, taken from Fig. 5(a). For wavelengths between 600 and 900 nm, a stronger driving field leads to a larger EQE enhancement; a similar trend also seen experimentally in Fig. 7(a).

Beyond a wavelength of 900 nm, the difference in the driving field intensity, and hence Q_{scat}, reduces as $|E_d|^2$ converges to 1.97 on bare Si, and 2.43 on an oxide. For example, at a wavelength of 1050 nm we can estimate that the Q_{scat} is 38% larger on the oxide (from the ratio of $|E_d|^2 = 2.64/1.92$). Additionally, at longer wavelengths the absorption coefficient of Si reduces, and multiple passes across the 2 μm active area are needed for the light to be absorbed. In this spectral region, the coupling efficiency becomes more important, as a fraction 1-F_{subs} of the light will be coupled out and lost at each scattering event. From Fig. 6, F_{subs} is lower for particles on a spacer layer for all wavelengths. Taking the example above, at a wavelength of 1050 nm, F_{subs} is 6% lower for particles on an oxide (from Fig. 6). We can estimate the path length enhancement of weakly absorbed light in the Si from, $PL = 2d_{ave}/(1\text{-}F_{subs})$, where d_{ave} is the distance traveled by the scattered light in one pass of the solar cell. We can estimate d_{ave} for the particles by calculating the d_{ave} of an emitting dipole above a Si substrate with an

equivalent value of $F_{subs,}$ as described in Ref. 13. The calculated path length enhancement is then 47% lower for particles on an oxide due to a 6% reduction in F_{subs}. The roughly similar trend in the experimental EQE enhancements for both cases above 900 nm in Fig. 7 are attributed to the combination of a higher Q_{scat} and a reduced F_{subs} for particles on an oxide.

Figure 7(b) shows the experimental EQE enhancements due to rear located particles. In this case, the particles on the bare Si provide a larger enhancement than the particles on the oxide at all wavelengths above 600 nm. At a wavelength of 1050 nm, the enhancement factor for particles on oxide is 3.2 while on the bare Si it is 4.5. This is due to the fact that particles directly on the Si have a roughly 30% larger Q_{scat} for all wavelengths, from Fig. 5(b). Coupled with a higher F_{subs}, shown in Fig. 6, this leads to larger EQE enhancements for particles directly on Si for all wavelengths.

We will now focus on the shorter wavelength regions from 400 to 600 nm. In this region, for front located particles in Fig. 7(a) we see photocurrent suppression due to interference between scattered and incident light.[19] We can see that there is a crossover point, at which the enhancement from the nanoparticles is equal to 1, as it changes from suppression to enhancement. Experimentally, this occurs at 500 nm for the oxide case and 650 nm for the bare Si case. This is not seen for rear located particles as the light is absorbed in the substrate before reaching the particles.

To investigate the effects of interference due to particle scattering for particles on the front, we can calculate the amount of light transmitted into the Si with and without a particle present using the same simulations setup described previously. Figure 8 shows the transmission enhancement, calculated as transmission with a front-located, 150 nm diameter particle, normalized to transmission in a reference case without a nanoparticle. The calculated crossover points occur at wavelengths of 610 nm for the oxide case (red, crosses), and 922 nm for the bare Si case (blue, circles).

Experimentally the crossover point in EQE enhancement for the particles on the bare Si [Fig. 7(a)] is substantially blue shifted compared to the calculated case, from 922 to 650 nm.

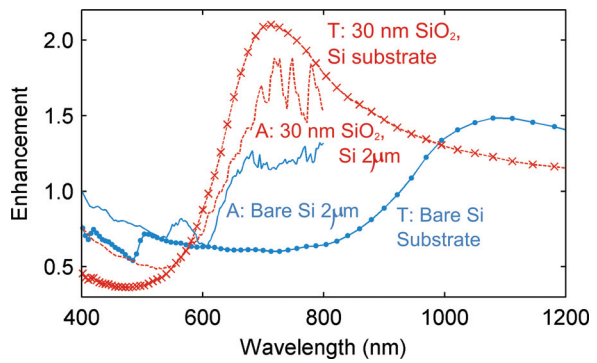

FIG. 8. (Color online) Enhancement in transmission (light into Si) in a semi-infinite Si substrate, calculated as transmission with a front-located, 150 nm diameter particle, normalized to a reference case with no particle present. The absorption enhancement in a 2 μm Si substrate is also plotted, calculated as the absorption in the Si with periodic nanoparticle arrays present normalized to the absorption in a 2 μm Si slab. Data is shown for particles on bare Si (with only a native oxide present) and for particles on a 30 nm oxide spacer layer.

This is because experimentally the particles are on a finite substrate and the EQE enhancement is due to a combination of the enhancement of the power transmitted into the Si and the fact that the light is scattered at high angles and trapped inside the Si. We will explain this now in more detail.

The amount of light trapping provided by the particles at a particular wavelength depends on the thickness of the substrate. For a 2 μm Si substrate, transmission losses exceed 10% at a wavelength of 500 nm. For wavelengths longer than this we can clearly see interference fringes in the EQE enhancement data in Figs. 7(a) and 7(b) due to interference between incident light and light that is reflected back from the rear interface. At these wavelengths light scattered outside the loss cone by the particles will travel multiple passes through the substrate and will have a greater chance of being absorbed, leading to enhanced EQE. We can clearly see this happening for particles on the rear, where photocurrent suppression is avoided: here both cases have enhanced EQE at wavelengths above 500 nm due to light trapping.

In order to calculate the effect of the combined light trapping and transmission enhancement (and photocurrent suppression) due to front located particles in our simulations we need to model finite, 2 μm thick Si substrates. For the finite substrate calculation the single particle approximation is no longer valid. Light scattered by the particle and totally internally reflected at the rear surface of the finite substrate will be reflected outside the simulation volume and so the increased path length will not contribute to increased absorption. Instead, we use periodic boundary conditions, to simulate a periodic array of nanoparticles. Here we measure the absorption as the difference between the transmission inside the Si, 100 nm from the front surface and 100 nm from the rear surface. In order for light scattered by a periodic array to be trapped it must be coupled into higher diffracted orders that propagate outside the loss cone in Si. The length of the period determines the number of diffracted orders that exist in the substrate. For small periods, only the zeroth order (which propagates normal to the surface) is present, while for larger periods higher diffracted orders are also present. The period hence determines the possibility of light trapping.[27] We choose a period of 240 nm to ensure a realistic surface coverage for 150 nm diameter particles, while still allowing light trapping to occur up to wavelengths of 850 nm.

The absorption enhancement is also plotted in Fig. 8, calculated as the absorption in the 2 μm Si substrate with periodic nanoparticle arrays on the front, normalized to the absorption for a plain substrate. The results were smoothed using a method of averaging that accounts for the variation of the interference fringes with wavelength.[28] The results are plotted up to a wavelength of 800 nm as higher (nonzero) diffracted orders only exist below wavelengths of 850 nm. The amount of light coupled into higher diffracted orders will gradually reduce up to this wavelength. Hence these simulations do not give us a quantitative prediction of the amount of light trapping provided by random arrays at long wavelengths. They are useful, however, as they show us the relative importance of light trapping and transmission enhancement. For the particles on 30 nm oxide, the single particle transmission enhancements agree well with the absorption enhancements in 2 μm of Si. This is because

photocurrent suppression due to interference occurs at wavelengths where light is absorbed in one pass across the 2 μm film and light trapping does not occur. For particles on bare Si, the region of photocurrent suppression, shown in the single particle transmission enhancements, occurs over a wide wavelength range up to 922 nm, while in the crossover point for absorption enhancement in 2 μm of Si occurs at a wavelength of 625 nm. At wavelengths above 500 nm transmission losses begin to occur and enhancements due to light trapping begin to become important. Above a wavelength of 625 nm the light trapping compensates for the suppressed transmission and leads to an overall enhancement in absorption. In other words, although less light is transmitted into the Si at these wavelengths due to the presence of the particles, the fact that it is scattered at high angles and trapped will increase the absorption overall. The absorption enhancement results agree well with the crossover points seen experimentally.

This means that for light trapping with the random particle arrays seen experimentally, the strength of the driving field is more important than the resonance position for particles on the front, leading to larger overall enhancements as the spacer layer is increased. This result is only true for random nanoparticle arrays with large size and shape distributions which have very broad resonances. Random arrays of uniform particles, deposited in a colloidal solution for example, will have narrower scattering resonances meaning that long wavelength enhancements will be reduced as the resonances are blue-shifted with increasing spacer layer thickness. Additionally, there is a trade off between the benefits of increased scattering and reductions in the coupling efficiency as the particle is moved further away from the Si substrate. Finally, we observe reduced transmission of incident light into the Si for cells with front located particles, due to interference effects. We have shown that the light trapping provided by the front located particles can overcome the suppression of the transmission to result in overall EQE enhancements. However, this only occurs when the reduced transmission is present at wavelengths where light trapping occurs, and this depends on cell and spacer layer thickness. For 2 μm Si cells, the particles that perform the best on 30 nm oxide layers, still suffer from photocurrent suppression at wavelengths in the blue-green region.

If particles are located on the rear of a solar cell, photocurrent suppression is completely avoided and light trapping and anti-reflection can be optimized independently.[21] In this case, particles directly on the Si provide both the largest scattering cross sections and coupling efficiencies, and hence the largest EQE enhancements, when compared to the case with oxide layers. This result can be extended more generally to cells that require passivation, as high index layers like a-Si, can provide passivation while maintaining high scattering and coupling efficiencies.

VI. CONCLUSION

The spacer layer thickness is an important parameter that needs to be considered separately for front and rear located particles when designing plasmonic solar cells. We have demonstrated that, for self-assembled Ag particles on the front, illuminated surface of solar cells, thin layers ($\sim$30 nm) of oxide are desirable to reduce photocurrent suppression at optical frequencies and increase the strength of the driving field, while still providing light trapping near the bandgap of Si due to the broad scattering resonances of the random nanoparticle arrays. However, on the rear of the solar cells, the nanoparticle arrays provide the most effective light trapping when deposited directly on the Si, due to enhanced scattering cross sections and coupling efficiencies.

ACKNOWLEDGMENTS

This work has been supported by the Australian Solar Institute (ASI). The ARC Photovoltaic Centre of Excellence is supported by the Australian Research Council's Centre of Excellence Scheme. K.R.C. acknowledges the support of an Australian Research Council fellowship and the EU FP7 PRIMA project. The authors would like to thank Dr. Patrick Campbell for the sputtered oxide layers used in this study.

[1]H. Atwater and A. Polman, Nat. Mater. **9**, 205 (2010).
[2]S. Pillai, K. R. Catchpole, T. Trupke, and M. A. Green, J. Appl. Phys. **101**, 093105 (2007).
[3]K. Nakayama, K. Tanabe, and H. A. Atwater, Appl. Phys. Lett. **93** 121904 (2008).
[4]A. J. Morfa, K. L. Rowlen, T. H. Reilly III, M. J. Romero, and J. v. d. Lagemaatb, Appl. Phys. Lett. **92**, 013504 (2008).
[5]A. V. Kabashin, P. Evans, S. Pastkovsky, W. Hendren, G. A. Wurtz, R. Atkinson, R. Pollard, V. A. Podolskiy, and A. V. Zayats, Nat. Mater. **8**, 867 (2009).
[6]S. Pillai, K. R. Catchpole, T. Trupke, G. Zhang, J. Zhao, and M. A. Green, Appl. Phys. Lett. **88**, 161102 (2006).
[7]J. Mertz, J. Opt. Soc. Am. B **17**(11), 1906 (2000).
[8]P. Royer, J. P. Goudonnet, R. J. Warmack, and T. L. Ferrel, Phys. Rev. B **35**(8), 3753 (1987).
[9]M. D. Malinsky, K. L. Kelly, G. C. Schatz, and R. P. Van Duyne, J. Phys. Chem. B **105**, 2343 (2001).
[10]F. J. Beck, A. Polman, and K. R. Catchpole, J. Appl. Phys. **105**, 114310 (2009).
[11]F. J. Beck, S. Mokkapati, A. Polman, and K. R. Catchpole, Appl. Phys. Lett. **96**, 033113 (2010).
[12]K. H. Drexhage, J. Lumin. **1–2**, 693 (1970).
[13]K. R. Catchpole and A. Polman, Appl. Phys. Lett. **93**, 191113 (2008).
[14]P. Matheu, S. H. Lim, D. Derkacs, C. McPheeters, and E. T. Yu, Appl. Phys. Lett. **93**, 113108 (2008).
[15]H. R. Stuart and D. G. Hall, Appl. Phys. Lett. **69**(16), 2327 (1996).
[16]W. R. Holland and D. G. Hall, Phys. Rev. B **27**, 7765 (1983).
[17]B. J. Soller and D. G. Hall, J. Opt. Soc. Am. A **18**(10), 2577 (2001).
[18]C. Hägglund, M. Zäch, G. Petersson, and B. Kasemo, Appl. Phys. Lett. **92**, 053110 (2008).
[19]S. H. Lim, W. Mar, P. Matheu, D. Derkacs, and E. T. Yu, J. Appl. Phys. **101**, 104309 (2007).
[20]Z. Ouyang, S. Pillai, F. Beck, O. Kunz, S. Varlamov, K. R. Catchpole, P. Campbell, and M. A. Green, Appl. Phys. Lett. **96**, 261109 (2010).
[21]F. J. Beck, S. Mokkapati, and K. R. Catchpole, Progr. Photovoltaics **18**, 1 (2010).
[22]O. Kunz, Z. Ouyang, J. Wong, and A. G. Aberle, Adv. OptoElectron. **2008**, 532351.
[23]See www.lumerical .com for software details, FDTD Solutions, Lumerical Solutions, Inc., Vancouver, 2003–2010.
[24]P. B. Johnson and R. W. Christy, Phys. Rev. B **6**(12), 4370 (1972).
[25]M. J. Keevers and M. A. Green, Appl. Phys. Lett. **66**(2), 174 (1995).
[26]E. D. Palik, *Handbook of Optical Constants of Solids* (Academic, New York, 1998).
[27]S. Mokkapati, F. J. Beck, A. Polman, and K. R. Catchpole, Appl. Phys. Lett. **95**, 053115 (2009).
[28]The data was smoothed by applying multiple averaging functions. Copies of the raw data were smoothed by averaging over different numbers of points from 2% to 10% of the total number of points. The different averaged data was then summed and the mean was taken. This method was tested with transmission data from planar substrates to ensure the data was well represented.